

## Hybrid metal/Ga<sub>2</sub>O<sub>3</sub>/GaN ultraviolet detector for obtaining low dark current and high responsivity

GUANSEN HUANG,<sup>1,2</sup> CHUNSHUANG CHU,<sup>1,3,5</sup> LONG GUO,<sup>4</sup> ZUPIN LIU,<sup>1,2</sup> KE JIANG,<sup>4</sup>  YONGHUI ZHANG,<sup>1,2</sup>  XIAOJUAN SUN,<sup>4</sup> ZI-HUI ZHANG,<sup>1,2,6</sup>  AND DABING LI<sup>4</sup>

<sup>1</sup>State Key Laboratory of Reliability and Intelligence of Electrical Equipment, 5340 Xiping Road, Beichen District, Tianjin, 300401, China

<sup>2</sup>School of Electronics and Information Engineering, Hebei University of Technology, Key Laboratory of Electronic Materials and Devices of Tianjin, 5340 Xiping Road, Beichen District, Tianjin, 300401, China

<sup>3</sup>School of Electrical Engineering, Hebei University of Technology, 5340 Xiping Road, Beichen District, Tianjin, 300401, China

<sup>4</sup>State Key Laboratory of Luminescence and Applications, Changchun Institute of Optics, Fine Mechanics and Physics, Chinese Academy of Sciences, Changchun, 130033, China

<sup>5</sup>e-mail: chuchunshuang@hotmail.com

<sup>6</sup>e-mail: zh.zhang@hebut.edu.cn

Received 31 January 2022; revised 15 February 2022; accepted 16 February 2022; posted 17 February 2022; published 15 March 2022

In this work, we have proposed and fabricated a metal/Ga<sub>2</sub>O<sub>3</sub>/GaN hybrid structure metal-semiconductor-metal ultraviolet photodetector with low dark current and high responsivity. The Schottky contact of Ni/Ga<sub>2</sub>O<sub>3</sub> makes the Ga<sub>2</sub>O<sub>3</sub> layer fully depleted. The strong electric field in the Ga<sub>2</sub>O<sub>3</sub> depletion region can push the photo-induced electrons from the Ga<sub>2</sub>O<sub>3</sub> layer into the GaN layer for more efficient carrier transport. Therefore, the hybrid structure simultaneously utilizes the advantage of the absorption to solar-blind ultraviolet light by the Ga<sub>2</sub>O<sub>3</sub> layer and the high electron mobility of the GaN layer. Thus, the dark current and the photocurrent for the proposed device can be greatly improved. As a result, an extremely high photo-to-dark-current ratio of  $1.46 \times 10^6$  can be achieved. Furthermore, quick rise and fall times of 0.213 s and 0.027 s at the applied bias of 6 V are also obtained, respectively. © 2022 Optica Publishing Group

<https://doi.org/10.1364/OL.454717>

In recent years, for ozone protection, missile warnings, and chemical/biological agent sensing in, e.g., public health, biosecurity, and confidential space communication, an increasing demand has been triggered for solar-blind UV photodetectors (PDs) [1]. Among alternative semiconductor materials, such as AlGaN and SiC for solar-blind UV PDs,  $\beta$ -Ga<sub>2</sub>O<sub>3</sub> has superior chemical and thermal stability. Moreover, its bandgap of 4.9 eV possesses an absorption cut-off edge of 280 nm [2], and this enables better detection of solar-blind UV light. However, the low electron mobility of Ga<sub>2</sub>O<sub>3</sub> at room temperature of 153 cm<sup>2</sup>/V·s at most strongly limits the carrier transport and the photocurrent [3]. On the other hand, at the current stage, Ga<sub>2</sub>O<sub>3</sub> material has promising prospects in fabricating metal-semiconductor-metal (MSM) PDs with two Schottky contacts [4]. Nevertheless, one of the bottlenecks limiting the responsivity for MSM PDs is the carrier transport [5]. A high-efficiency carrier transport can be achieved by increasing the electric field magnitude in the absorption region, i.e., a strong electric field

can be even generated at the equilibrium state. This is achievable if an asymmetric energy band can be made between the two Schottky contacts [6]. In most cases, such an asymmetric energy band can be obtained by using two metal contacts with different work functions [7]. According to our most recent report, an even stronger electric field in the absorption region can be obtained by using the polarized AlGaN/GaN junction [8]. Besides, the electric field in the optical absorption region can also be tuned by using the energy band offset [9], e.g., based on the Ga<sub>2</sub>O<sub>3</sub> material system, Ga<sub>2</sub>O<sub>3</sub>/SiC and ZnO/Ga<sub>2</sub>O<sub>3</sub> heterostructures have been developed [10,11]. These heterostructures can bend the energy band at the interface of the heterojunction, causing a depletion region and then generating an increased electric field. Although the built-in electric field accelerates the transport of carriers, the carrier transport paths are mainly in the Ga<sub>2</sub>O<sub>3</sub> layer. Meanwhile, the carriers in the Ga<sub>2</sub>O<sub>3</sub> layer are easily trapped by local lattice defects [3], which strongly reduce the photocurrent.

In order to reduce the influence of the defects in the Ga<sub>2</sub>O<sub>3</sub> region on the performance for Ga<sub>2</sub>O<sub>3</sub>-based MSM PDs, in this work, we have designed a hybrid Ni/Ga<sub>2</sub>O<sub>3</sub>/GaN-based MSM PD structure, such that the Ga<sub>2</sub>O<sub>3</sub> layer is adopted to absorb UV photons. The energy band bending profiles for the Ni/Ga<sub>2</sub>O<sub>3</sub>/GaN heterostructure enable the photo-generated electrons to enter the GaN layer for transport. Our tested results show that the better electron mobility in the GaN layer favors the reduced time during the UV-on and UV-off processes for the proposed hybrid structure.

The epitaxial structure for our PDs is grown on a sapphire substrate by using the metal organic chemical vapor deposition (MOCVD) system. Firstly, a 20 nm thick GaN layer is utilized as a buffer layer. Then, a 2  $\mu$ m thick unintentionally n-type GaN layer is grown (u-GaN) and the electron concentration is estimated to be  $1.0 \times 10^{16}$  cm<sup>-3</sup>. This layer functions as the carrier transport layer. Then, the GaN wafer is transferred to another MOCVD system and 100 nm thick  $\beta$ -Ga<sub>2</sub>O<sub>3</sub> layer is capped on the u-GaN layer.

A schematic diagram for the fabricated hybrid Ni/Ga<sub>2</sub>O<sub>3</sub>/GaN UV PD is shown in Fig. 1(a). The device fabrication process is

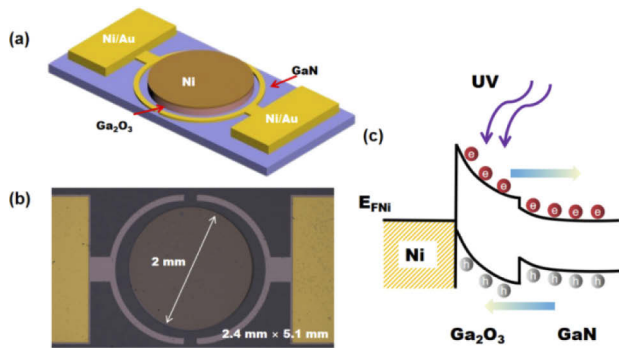


**Fig. 1.** (a) Schematic device structure for the hybrid Ni/Ga<sub>2</sub>O<sub>3</sub>/GaN UV PD. (b) Top view for the fabricated Ni/Ga<sub>2</sub>O<sub>3</sub>/GaN UV PD. (c) Schematic illustration of the bandgap alignment for the Ni/Ga<sub>2</sub>O<sub>3</sub>/GaN junctions.

as follows. After the epitaxial growth, the  $\beta$ -Ga<sub>2</sub>O<sub>3</sub> is dry etched by using an inductively coupled plasma (ICP) etching system to form the circular  $\beta$ -Ga<sub>2</sub>O<sub>3</sub> mesa with a diameter of 2 mm, as presented in Fig. 1(b). Ni/Au (5 nm/5 nm) is deposited on the  $\beta$ -Ga<sub>2</sub>O<sub>3</sub> mesa by utilizing an e-beam system. The two Ni/Au (10 nm/10 nm) Schottky contacts are deposited around the  $\beta$ -Ga<sub>2</sub>O<sub>3</sub> mesa. Then, we deposit a 200 nm thick Au layer on the Ni/Au metal stacks for the device test. Figure 1(c) illustrates the schematic energy band diagram for the Ni/Ga<sub>2</sub>O<sub>3</sub>/GaN structure. The electron affinity for Ni with 5.15 eV is larger than that for Ga<sub>2</sub>O<sub>3</sub> with 4.0 eV [12]. Therefore, the built-in electric field will be generated in the Ni/Ga<sub>2</sub>O<sub>3</sub> junction and the energy band profile for the Ga<sub>2</sub>O<sub>3</sub> layer will make the photo-generated electrons move to the GaN region from the Ga<sub>2</sub>O<sub>3</sub> layer. In addition, the conduction band offset for the GaN/Ga<sub>2</sub>O<sub>3</sub> heterojunction is  $\Delta E_c = 0.1$  eV [13] and this further makes the photo-generated electrons transport from the Ga<sub>2</sub>O<sub>3</sub> to the GaN.

To better understand the device physics and the carrier transport process, numerical simulations are conducted by using APSYS. The Shockley–Read–Hall (SRH) recombination lifetime is set to 10 ns [14]. The electron affinity for the Ni layer is set to 5.15 eV [12]. The energy band gaps for Ga<sub>2</sub>O<sub>3</sub> and GaN materials are set to 4.9 eV and 3.4 eV, respectively [13]. The conduction band offset and the valence band offset at the Ga<sub>2</sub>O<sub>3</sub>/GaN interface are 0.10 eV and 1.40 eV, respectively [13]. The optical absorption coefficient for Ga<sub>2</sub>O<sub>3</sub> and GaN materials in terms of the wavelength are also considered according to Peeelaers and Van de Walle [15] and Muth *et al.* [16], respectively. Other physical parameters for Ga<sub>2</sub>O<sub>3</sub> and GaN materials can be found elsewhere [17,18].

We have measured the X-ray diffraction (XRD) rocking curves ( $\omega$ -scans) of asymmetric planes for Ga<sub>2</sub>O<sub>3</sub>, as shown in Fig. 2(a).

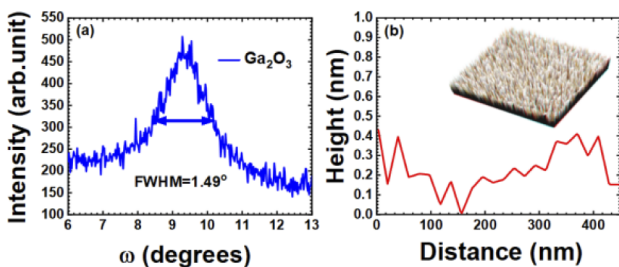


**Fig. 2.** (a) High-resolution XRD rocking curve for the Ga<sub>2</sub>O<sub>3</sub> film. (b) AFM image of the surface conditions for the Ga<sub>2</sub>O<sub>3</sub> film.

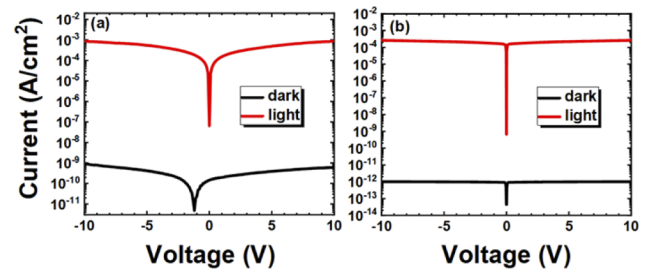


**Fig. 3.** Dark and photocurrent density in terms of the applied bias from (a) experimental measurement and (b) numerical calculations.

The full width at half maximum (FWHM) for the  $(-201)$ -planed Ga<sub>2</sub>O<sub>3</sub> is 1.49°. This is consistent with the previously reported results [19], which indicates that the grown Ga<sub>2</sub>O<sub>3</sub> layer has excellent crystalline quality. The surface morphology for the Ga<sub>2</sub>O<sub>3</sub> film deposited on the GaN layer is measured by using an atomic force microscope (AFM). Figure 2(b) shows that the surface roughness fluctuation is smaller than 0.5 nm. Moreover, the inset of Fig. 2(b) shows the three-dimensional (3D) AFM image with a scanning area of  $1 \times 1 \mu\text{m}^2$ . The root-mean-square (RMS) surface roughness is 0.144 nm. Hence, the Ga<sub>2</sub>O<sub>3</sub> film deposited on the GaN surface possess smooth surface morphology.

Figure 3(a) exhibits the measured dark current and the photocurrent in terms of the applied bias for the fabricated Ni/Ga<sub>2</sub>O<sub>3</sub>/GaN MSM UV PD. At the applied bias of 10 V, the dark current is smaller than  $0.1 \text{ A/cm}^2$  and the photocurrent is larger than  $10^{-3} \text{ A/cm}^2$  when the intensity for the UV signal is  $435 \mu\text{W/cm}^2$ , rendering a detectivity of  $1.43 \times 10^{14}$  Jones. As a result, the ratio between the photocurrent and the dark current ( $I_{PC}/I_{DC}$ ) for our proposed device reaches a high level of  $1.46 \times 10^6$ . The numerically calculated dark current and the photocurrent as a function of the applied bias are presented in Fig. 3(b). Note, the calculated current level is smaller than the measured one, and this might be caused by the unoptimized trap information in our models. However, this does not affect our conclusion that the photocurrent for our proposed PD structure can be greatly enhanced.

We believe that the adoption of the Ni gate metal helps to deplete the electrons in the GaN layer. However, when the UV light is on, the photo-generated electrons in the Ga<sub>2</sub>O<sub>3</sub> layer are pushed into the GaN layer. Note, the increased electron concentration in the GaN layer will screen the built-in electric field generated in the Ni/Ga<sub>2</sub>O<sub>3</sub>/GaN junctions, and thus the electrons with increased mobility in the GaN layer favor the more efficient transport between the two Schottky contacts. For the purpose of in-depth discussion, numerical investigations will be conducted subsequently. The cross-sectional distribution of electron concentration for the proposed PD is shown in Fig. 4(a) when the UV light is not turned on. We observe that the whole Ga<sub>2</sub>O<sub>3</sub> layer has been depleted because of the built-in electric field at the Ni/Ga<sub>2</sub>O<sub>3</sub> junction. Figure 4(b) then presents the calculated energy band diagram at the applied bias of 6 V. It agrees with Fig. 4(a), such that the energy band profile in the Ga<sub>2</sub>O<sub>3</sub> layer indicates a strong electron depletion effect therein. Meanwhile, in the range of  $0.10 \mu\text{m}$  and  $0.60 \mu\text{m}$ , the electrons in the GaN layer are also depleted. Hence, few electrons participate in the contribution of generating dark current, which is interpreted as causing the very low dark current in Fig. 3. When the 254 nm UV light source is applied to the top of the device, as shown in Fig. 4(c), we observe that the built-in electric field in the

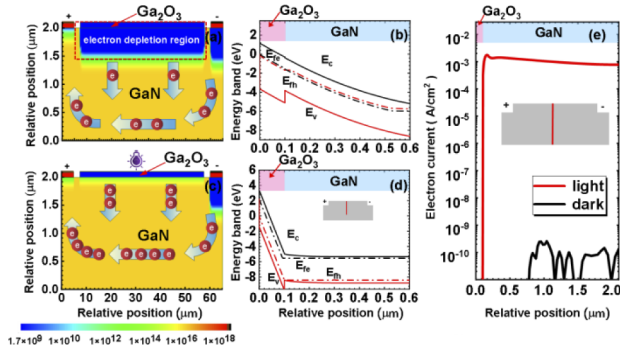


**Fig. 4.** (a) 2D profiles of the electron concentration for the proposed PD in the case of no UV light illumination. (b) The energy band alignment for the Ga<sub>2</sub>O<sub>3</sub>/GaN junction in the case of no UV light illumination. (c) 2D profiles of the electron concentration for the proposed PD in the case of UV light illumination. (d) The energy band alignment for the Ga<sub>2</sub>O<sub>3</sub>/GaN junction in the case of UV light illumination. (e) Electron current profiles when the UV light is on and off. Here,  $E_c$ ,  $E_v$ ,  $E_{fe}$ , and  $E_{fh}$  represent the conduction band, valence band, and quasi-Fermi levels of electrons and holes, respectively. The data are calculated at the bias of 6 V.

**Table 1.  $I_{PC}/I_{DC}$  Ratio for the Reported  $\beta$ -Ga<sub>2</sub>O<sub>3</sub> Film-Based MSM UV PDs in the Literature**

Material	Dark Current (A)	Photo-to-Dark Ratio	References
Ga <sub>2</sub> O <sub>3</sub> /GaN	$1.6 \times 10^{-10}$ (10 V)	1375 (10 V, 8000 $\mu\text{W}/\text{cm}^2$ )	[20]
Ga <sub>2</sub> O <sub>3</sub> /GaN	$7.25 \times 10^{-10}$ (0 V)	272.15 (10 V, 2400 $\mu\text{W}/\text{cm}^2$ )	[21]
Ga <sub>2</sub> O <sub>3</sub> /GaN	$<1 \times 10^{-9}$ (8 V)	$\approx 500$ (2 V, 22,000 $\mu\text{W}/\text{cm}^2$ )	[2]
Ga <sub>2</sub> O <sub>3</sub> /GaN	$>1 \times 10^{-5}$ (40 V)	$>100$ (40 V, 6700 $\mu\text{W}/\text{cm}^2$ )	[19]
Sn:Ga <sub>2</sub> O <sub>3</sub> /GaN	$1.8 \times 10^{-11}$ (0 V)	$\approx 10^4$ (0 V, 1000 $\mu\text{W}/\text{cm}^2$ )	[22]
Ga <sub>2</sub> O <sub>3</sub>	70 (20 V)	45 (20 V)	[23]
Nanoporous-GaN/Ga <sub>2</sub> O <sub>3</sub>	$2.8 \times 10^{-5}$ (5 V)	39.28 (5 V, 2.44 $\mu\text{W}/\text{cm}^2$ )	[24]
Ni/Ga <sub>2</sub> O <sub>3</sub> /GaN	$1.9 \times 10^{-11}$ (10 V)	$1.46 \times 10^6$ (10 V, 435 $\mu\text{W}/\text{cm}^2$ )	This work <sup>a</sup>

<sup>a</sup>The unit of ampere for dark current is used for comparison by considering the circular mesa with the diameter of 2 mm.

Ni/Ga<sub>2</sub>O<sub>3</sub> junction fully pushes the photo-generated electrons in the Ga<sub>2</sub>O<sub>3</sub> layer into the GaN layer. Figure 4(d) then shows the calculated energy band diagram at the applied bias of 6 V, and it illustrates that the electrons are stored in the GaN layer, which agrees with the observations in Fig. 4(c). Considering the larger electron mobility in the GaN material, the electron transport between the two Schottky contacts is more efficient and the photocurrent for our proposed PD correspondingly becomes increased, as shown in Fig. 3. Figure 4(e) demonstrates the spatial distributions for the electron current in the GaN layer when the UV light is off and on. It shows that the photo-generated electron current is mainly confined in the GaN layer, and the ratio between the photo-generated electron current and the dark electron current is as high as  $10^6$  in Fig. 4(e). This number is consistent with the  $I_{PC}/I_{DC}$  ratio in Table 1.

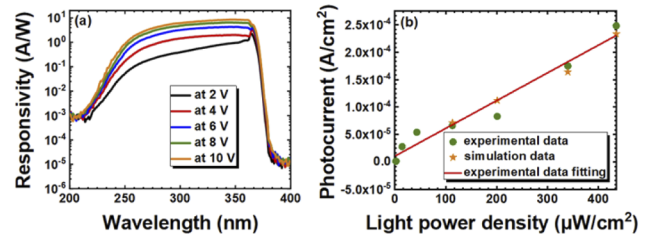


**Fig. 5.** (a) Spectral responsivity in terms of the incident light wavelength at different applied biases. Legend in inverse order of curves. (b) Experimentally measured and numerically calculated relationship between the light power intensity and the photocurrent at the applied bias of 2 V.

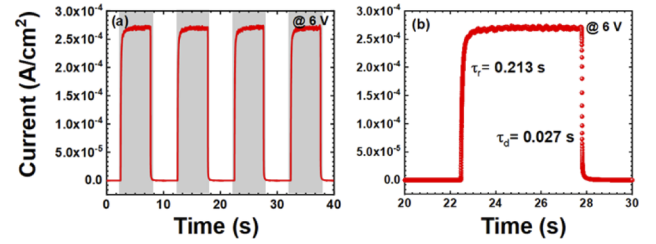


**Fig. 6.** Time-dependent optical response in (a) multiple cycles and (b) a single cycle when a 254 nm UV illumination signal is applied. The bias is set to 6 V.

The responsivity as a function of the wavelength for the proposed PD is measured and presented in Fig. 5(c). The responsivity increases as the applied bias on the Schottky contact becomes large. The responsivity shows a sharp increase when the wavelength increases from 200 nm to 250 nm, which denotes the optical absorption by the Ga<sub>2</sub>O<sub>3</sub> layer [2]. However, the responsivity in the near UV range is also observed, and this may arise from the possible fact that the Ga<sub>2</sub>O<sub>3</sub> layer thickness shall be further increased to be beyond 100 nm so that more effective optical absorption can be achieved. Figure 5(b) demonstrates the relationship between the incident light intensity and photocurrent at the applied bias of 2 V. It can be seen that the photocurrent increases linearly with the incident light power, in spite of the small applied bias. Moreover, the numerically simulated data agree well with the experimentally measured data, which also confirms the validity of the physical models. The absence of the saturation of the photo-generated current in terms of the incident light power density indicates the high-efficiency carrier transport between the two Schottky contacts [25].

It is well known that the response speed of PDs is strongly related to the carrier transport and carrier collection efficiency. Thus, the multiple-cycle time-dependent optical response for the studied device is measured at the applied bias of 6 V, as shown in Fig. 6(a). For better illustration, the time-dependent optical response for a single cycle is shown in Fig. 6(b). A rise time ( $\tau_r$ ) of 0.213 s and a decay time ( $\tau_d$ ) of 27 ms can be obtained for the proposed PD in this work. Here,  $\tau_r$  is defined as the time interval when the photocurrent increases from 10 to 90% of its peak value, and  $\tau_d$  is defined as the time interval when the photocurrent decreases from 90 to 10% of its peak value [26]. Table 2 summarizes the reported rise time and the decay time for different Ga<sub>2</sub>O<sub>3</sub>-based PDs. The comparison shows that our proposed PD has a much shorter decay time when compared with others. The rise time is also at an excellent level. However,

**Table 2. Response Times for the Reported Ga<sub>2</sub>O<sub>3</sub>-Based MSM UV PDs**

Material	Rise and Decay Time (s)	Method	References
Ga <sub>2</sub> O <sub>3</sub>	2.97/0.41 (10 V)	MBE <sup>a</sup>	[30]
Ga <sub>2</sub> O <sub>3</sub>	5.0/10.3 (20 V)	MBE	[23]
Ga <sub>2</sub> O <sub>3</sub>	0.41/0.04 (10 V)	MBE	[31]
SiC/Ga <sub>2</sub> O <sub>3</sub>	0.65/0.04 (5 V)	MOCVD	[10]
Ga <sub>2</sub> O <sub>3</sub>	0.58/1.2 (10 V)	MOCVD	[32]
Ga <sub>2</sub> O <sub>3</sub> /GaN	0.14/0.16 (2 V)	MOCVD	[21]
Nanoporous-GaN/Ga <sub>2</sub> O <sub>3</sub>	1.09/0.79 (10 V)	MBE	[24]
Ni/Ga <sub>2</sub> O <sub>3</sub> /GaN	0.213/0.027 (6 V)	MOCVD	This work

<sup>a</sup>MBE, molecular beam epitaxy.

we believe the rise time can be even shorter if the number of electron traps in the Ga<sub>2</sub>O<sub>3</sub> layer can be further reduced [27] or an AlGaN/GaN-based structure for electron transport is utilized [28,29]. Note, although the built-in electric field can be generated in the Ni/Ga<sub>2</sub>O<sub>3</sub> junction, these traps will prevent the photo-generated electrons from being transported from the Ga<sub>2</sub>O<sub>3</sub> layer to the GaN layer when the UV light is turned on.

In conclusion, we have fabricated and demonstrated a hybrid Ni/Ga<sub>2</sub>O<sub>3</sub>/GaN UV PD. The Ni/Ga<sub>2</sub>O<sub>3</sub> junction can induce a strong electrical field that bends the energy band and depletes the background electrons. This helps to reduce the dark current for this proposed device. Moreover, the Ni/Ga<sub>2</sub>O<sub>3</sub>/GaN junctions also enable the photo-generated electrons in the Ga<sub>2</sub>O<sub>3</sub> layer to be transported into the GaN layer. Then, a more effective carrier transport can be favored in the GaN region, and thus a very high  $I_{PC}/I_{DC}$  ratio of  $1.46 \times 10^6$  can be generated. Thanks to the high carrier mobility in the GaN layer, the fabricated UV PD also demonstrates reduced rise time and decay time when a pulsed UV signal is applied. Therefore, we strongly believe that the reported structure provides a prototype device for the community to make high-performance UV detectors, and the device physics revealed here enrich the understanding of photo-sensitive devices.

**Funding.** National Natural Science Foundation of China (62074050, 61975051); Natural Science Foundation of Hebei Province (F2020202030); State Key Laboratory of Reliability and Intelligence of Electrical Equipment, Hebei University of Technology (EERI\_PI2020008, EERIPD2021012); Jiangsu Provincial Key Laboratory of Photonic and Electronic Materials Sciences and Technology, Nanjing University (njuzds2021-005).

**Disclosures.** The authors declare no conflicts of interest related to this paper.

**Data availability.** Data underlying the results presented in this paper are not publicly available at this time but may be obtained from the authors upon reasonable request.

## REFERENCES

- J. Xu, W. Zheng, and F. Huang, *J. Mater. Chem. C* **7**, 8753 (2019).
- S. Nakagomi, T. Sato, Y. Takahashi, and Y. Kokubun, *Sens. Act. A* **232**, 208 (2015).
- T. Oishi, Y. Koga, K. Harada, and M. Kasu, *Appl. Phys. Express* **8**, 031101 (2015).
- Y. Qin, L. Li, X. Zhao, G. S. Tompa, H. Dong, G. Jian, Q. He, P. Tan, X. Hou, Z. Zhang, S. Yu, H. Sun, G. Xu, X. Miao, K. Xue, S. Long, and M. Liu, *ACS Photonics* **7**, 812 (2020).
- Z. X. Jiang, Z. Y. Wu, C. C. Ma, J. N. Deng, H. Zhang, Y. Xu, J. D. Ye, Z. L. Fang, G. Q. Zhang, J. Y. Kang, and T.-Y. Zhang, *Mater. Today Phys.* **14**, 100226 (2020).
- Y. Zhi, Z. Liu, X. Chu, S. Li, Z. Yan, X. Wang, Y. Huang, J. Wang, Z. Wu, D. Guo, P. Li, and W. Tang, *ECS J. Solid State Sci. Technol.* **9**, 065011 (2020).
- Z. Liu, X. Wang, Y. Liu, D. Guo, S. Li, Z. Yan, C.-K. Tan, W. Li, P. Li, and W. Tang, *J. Mater. Chem. C* **7**, 13920 (2019).
- J. Wang, C. Chu, K. Tian, J. Che, H. Shao, Y. Zhang, K. Jiang, Z.-H. Zhang, X. Sun, and D. Li, *Photonics Res.* **9**, 734 (2021).
- D. Wang, X. Liu, Y. Kang, X. Wang, Y. Wu, S. Fang, H. Yu, M. H. Memon, H. Zhang, W. Hu, Z. Mi, L. Fu, H. Sun, and S. Long, *Nat. Electron.* **4**, 645 (2021).
- Y. Qu, Z. Wu, M. Ai, D. Guo, Y. An, H. Yang, L. Li, and W. Tang, *J. Alloys Compd.* **680**, 247 (2016).
- B. Zhao, F. Wang, H. Chen, L. Zheng, L. Su, D. Zhao, and X. Fang, *Adv. Funct. Mater.* **27**, 1700264 (2017).
- Z. Liu, Y. Zhi, S. Li, Y. Liu, X. Tang, Z. Yan, P. Li, X. Li, D. Guo, Z. Wu, and W. Tang, *J. Phys. D: Appl. Phys.* **53**, 085105 (2020).
- W. Wei, Z. Qin, S. Fan, Z. Li, K. Shi, Q. Zhu, and G. Zhang, *Nanoscale Res. Lett.* **7**, 562 (2012).
- Z.-H. Zhang, S.-W. Huang Chen, Y. Zhang, L. Li, S.-W. Wang, K. Tian, C. Chu, M. Fang, H.-C. Kuo, and W. Bi, *ACS Photonics* **4**, 1846 (2017).
- H. Peelaers and C. G. Van de Walle, *Appl. Phys. Lett.* **111**, 182104 (2017).
- J. F. Muth, J. D. Brown, M. A. L. Johnson, Z. Yu, R. M. Kolbas, J. W. Cook, and J. F. Schetzina, *MRS Internet J. Nitride Semicond. Res.* **4**, 502 (1999).
- M. Orita, H. Ohta, M. Hirano, and H. Hosono, *Appl. Phys. Lett.* **77**, 4166 (2000).
- Z. Alaie, S. Mohammad Nejad, and M. H. Yousefi, *Mater. Sci. Semicond. Process.* **29**, 16 (2015).
- A. Kalra, S. Vura, S. Rathkanthiwar, R. Muralidharan, S. Raghavan, and D. N. Nath, *Appl. Phys. Express* **11**, 064101 (2018).
- W. Ding and X. Meng, *J. Alloys Compd.* **866**, 157564 (2021).
- T. Chen, X. Zhang, Y. Ma, T. He, X. Wei, W. Tang, W. Tang, X. Zhou, H. Fu, L. Zhang, K. Xu, C. Zeng, Y. Fan, Y. Cai, and B. Zhang, *Adv. Photo Res.* **2**, 2100049 (2021).
- D. Guo, Y. Su, H. Shi, P. Li, N. Zhao, J. Ye, S. Wang, A. Liu, Z. Chen, C. Li, and W. Tang, *ACS Nano* **12**, 12827 (2018).
- L. X. Qian, Y. Wang, Z. H. Wu, T. Sheng, and X. Z. Liu, *Vacuum* **140**, 106 (2017).
- R. Meng, X. Ji, Z. Lou, J. Yang, Y. Zhang, Z. Zhang, W. Bi, J. Wang, and T. Wei, *Opt. Lett.* **44**, 2197 (2019).
- X. Chen, K. Liu, Z. Zhang, C. Wang, B. Li, H. Zhao, D. Zhao, and D. Shen, *ACS Appl. Mater. Interfaces* **8**, 4185 (2016).
- Y. Wang and N. Yu, *Mater. Express* **10**, 629 (2020).
- D. Guo, Z. Wu, P. Li, Y. An, H. Liu, X. Guo, H. Yan, G. Wang, C. Sun, L. Li, and W. Tang, *Opt. Mater. Express* **4**, 1067 (2014).
- K. Jiang, X. Sun, Z.-H. Zhang, J. Ben, J. Che, Z. Shi, Y. Jia, Y. Chen, S. Zhang, W. Lv, and D. Li, *Photonics Res.* **8**, 1243 (2020).
- H. Zhang, F. Liang, K. Song, C. Xing, D. Wang, H. Yu, C. Huang, Y. Sun, L. Yang, X. Zhao, H. Sun, and S. Long, *Appl. Phys. Lett.* **118**, 242105 (2021).
- L. X. Qian, H. Y. Liu, H. F. Zhang, Z. H. Wu, and W. L. Zhang, *Appl. Phys. Lett.* **114**, 113506 (2019).
- L.-X. Qian, Z.-H. Wu, Y.-Y. Zhang, P. T. Lai, X.-Z. Liu, and Y.-R. Li, *ACS Photonics* **4**, 2203 (2017).
- S. Oh, Y. Jung, M. A. Mastro, J. K. Hite, C. R. Eddy, and J. Kim, *Opt. Express* **23**, 28300 (2015).